Journal of Engineering Mathematics 19 (1985) 265–295.

A theory for vortex shedding from the keels of marine vehicles

D.T. BROWN and M.H. PATEL

Department of Mechanical Engineering, University College London, Torrington Place, London WC1E 7JE, England

(Received March 27, 1985)

Summary

This paper presents a discrete vortex-shedding method for predicting the damping forces experienced by a floating marine vehicle responding at and around roll resonance. The method utilizes a Schwartz-Christoffel transformation, the temporal flow development being calculated to yield vortex positions, pressures and overall forces on the vessel hull. The effect of the velocity term in Bernoulli's equation on hull forces is calculated by integrating pressure and confirmed using the Blasius formula. A functional form of the vortex-induced moment amplitude is deduced from the theory and applied to a frequency-domain equation of roll motion for the vessel. Comparison of theory with test data indicates that the vortex-shedding theory does predict the effects of this phenomenon on the roll motions of a specific hull shape. An extensive review of previous work in this area is also presented.

1. Introduction

Accurate predictions of the wave-induced roll motions of marine vehicles such as ships and barges are of considerable importance to effective design and operation of such vessels. A particular example of this is associated with the use of large ocean-going flat-bottomed barges in the offshore oil industry. These vessels are usually towed to their destination, and used for transporting bulky cargoes. During transportation the cargo structures are secured to the vessel deck with welded steel fastenings. The fastenings, and the cargo itself, have to be designed to withstand inertia forces due to barge motions, particularly roll, in a seaway. These roll motions can induce inertia loads that are often significantly higher than the maximum loads that the cargo may experience when in place. Thus both cargo modules and fastening designs are strongly dependent on accurate predictions of barge roll motions. The need for reliable data is further accentuated by the continuing trend towards larger vessels carrying heavier and more valuable cargoes for longer tows in open ocean conditions. Similar problems with ship roll motions are commonplace for a variety of applications.

Wave-exciting forces and motions of conventional floating vessels in gravity waves may be calculated using linear potential-flow theory, which neglects viscous effects that cause flow separation and skin-friction drag. Vessel motions and wave amplitudes are assumed to be very small for linear theory to apply. Experience has shown that linear theory gives realistic predictions of motions in the degrees of freedom that are heavily damped, but large discrepancies occur between calculations and test data for lightly damped motions, especially those of large amplitude. In particular, the roll motion of flat-bottomed barges

near resonance is considerably overestimated. This degree of freedom is particularily important, partly because it is difficult to predict, but also because it is responsible for inducing some of the severest accelerations experienced by the cargo, since typical barge-roll natural periods are within the range of predominant wave periods. A number of currently available motion-response calculation methods do include empirical estimates of damping forces due to viscous effects on the vessel submerged hull, but at present theoretically sound methods to calculate the precise influence of these phenomena do not exist.

The wave-induced motion response of a stationary freely floating marine vehicle, such as a barge, depends on its interaction with the surrounding fluid in a complex manner. The equations of motion must account for "added mass" and "damping" forces caused by induced accelerations in the surrounding fluid and the radiation of outwardly travelling gravity waves, due to body motions. These forces are predicted well by linear theory. However, a linear representation cannot account for other velocity-dependent forces that dissipate energy around the vessel keel. Apart from the linear mechanism of gravity-wave radiation mentioned previously, flows can also exist due to the unsteady boundary layer, its localised separations and associated vortex shedding. These phenomena are caused by relative motion between the local fluid and submerged vessel boundary, particularly near large changes of hull slope.

It is also possible that nonlinear wave forces could affect vessel motions, particularily if these are of large amplitude, such as at roll resonance. Discrepancies in roll motion between experiment and theory could be explained by a detuning at resonance caused by the nonlinear nature of wave loading on the vessel hull. This possibility is discussed further in Section 2.

This paper presents a detailed description of a method based on potential-flow point vortices to estimate forces and moments on the vessel due to vortex shedding from its keel. Results are presented for the flow development and vortex-induced loads. Experimental data are used to verify the results of the vortex-shedding method. It is believed that the test data yield a measure of the effects of vortex shedding only on the roll motions of the test vessel. A detailed review of previous work in this area is also presented.

2. Review of previous work

A review is presented in two parts, the first describing investigations of the roll motions of ship forms and the second dealing with applications of the discrete-vortex method (DVM) for modelling flows with vorticity.

2.1. Roll motions of floating bodies

Bilge keels, which are essentially flat plates or similar structures protruding outwards from the submerged vessel corners, have been commonly used to reduced the roll motions of floating vessels. Froude [1], one of the earliest workers in this area, realised that the total roll damping of a ship, with or without bilge keels, was not proportional to the square of the rate of rolling but was better represented by a combination of linear and square-law terms. Froude's hypothesis was based on experiments performed with a flat plate oscillating in water at various frequencies. Martin [2] extended these investigations to vary the amplitude of plate oscillation and concluded that the drag on the plate varied with amplitude to a power between 1 and 2.

White [3] performed experiments on battleships and found that the additional damping produced by fitting bilge keels was linear, rather than square law in character. He therefore concluded that surface wave radiation must be an important element in bilge-keel damping. Bryan [4] indicated that for ships with fairly large bilge keels, the transverse velocity of the water could be considerably greater than the product of the radius from the roll centre to the bilge keel and the rate of change of roll angle. Bryan also observed that when the ship was rolling, a pressure force would act on the hull ahead of each keel and a suction force behind it, these forces exerting a moment on the vessel that opposed the rolling motion. Other workers include Gawn [5] and Dalzell [6] who performed and analysed roll tests on battleships. They found that the test data fitted well to quadratic and cubic variations with roll amplitude.

Over the last two decades a large number of measurements have been made on the roll motions of ships by the 17th Research Committee of the Shipbuilding Research Association of Japan. Kato [7] developed a method using results of experiments that measured the resistance to rolling of immersed suspended cylinders, and concluded that the frictional damping of ships was insignificant compared to the dominant effects of wave damping. Tanaka [8] refined the experiments to measure the total resistance to rolling due to eddy making (shedding of vortices from the bilge keels) and friction and hence calculated the resistance due to eddy making alone by subtracting the effects of frictional resistance calculated by Kato's method.

Semi-empirical methods based on Tanaka's results have had varying degrees of success in predicting resonant roll motions. For example, Salvesen et al. [9] developed a method using strip theory and a representation of viscous damping, to predict vessel roll motions in significantly closer agreement with experimental measurements than the same theory gave without viscous damping. Tanaka has published further work with Ikeda and Himeno [10] which develops other semi-empirical formulae for the roll-damping terms due to friction, wave, eddy and lift components for the hull and bilge-keel contributions with no interaction accounted for between the various terms. The friction term was based on work by Blasius (see for example Newman [11]); the wave-damping term was calculated using strip theory; the eddy-making term was derived from earlier work by Ikeda et al. [12] on two-dimensional cylinders of various cross section (resulting in rather long and complicated formulae giving a result depending quadratically on roll frequency and amplitude); and the lift and bilge-keel contributions were both semi-analytical in nature, agreeing reasonably well with experimental results. The authors concluded that the sum of the five damping components showed good agreements with experimental results for ordinary ship forms. However, for ships with high breadth-to-draught ratios such as flat-bottomed barges this method was not always accurate.

Investigations into the motions of flat-bottomed barges have been carried out only recently as these vessels have now come into regular use due to the development of the offshore oil industry. Keuning and Beukelman [13] performed forced roll-oscillation tests to measure the added-mass and damping values of rectangular barges in various water depths, comparing the results with both a strip theory and diffraction model. They indicated that the effects of viscosity played an important role at high wave frequencies, where a growing amount of eddy shedding from the sharp corners could be observed. Surprisingly they found that the sway added-mass and damping coefficients remained independent of the oscillation amplitude even when there was much vortex shedding, though the roll coefficients were amplitude-dependent. Keuning and Beukelman concluded that the predicted damping coefficients were low, especially at higher frequencies

where viscous effects were dominant, the damping in roll being particularily difficult to estimate accurately.

Stewart, Ewers and Denton [14] arrived at similar conclusions after comparing roll-motion results for full and 1 : 30 scale models with predictions from commercially available computer programs. They indicated that the results of model tests showed that roll damping was a nonlinear phenomenon, the equation of motion being represented by

$$(I + I')\ddot{\theta} + B_1\dot{\theta} + B_2\dot{\theta}^3 + S\theta = F\cos(\omega t + \phi) \tag{1}$$

where I and I' are the roll inertia and added inertia, S the roll stiffness, F the roll-exciting force to waves of frequency ω, and B_1 and B_2 are constants. Stewart found that the barge roll response per metre wave amplitude decreased with increasing wave height due to increased damping forces and that, in general, the inability of programs to account accurately for the viscous damping in roll led to enormous variations in roll-motion predictions close to resonance. By considering an equation of the form of (1) a better representation of the roll motions could be found, though they did not know of any theoretical method that existed to calculate appropriate values of B_1 and B_2 for a particular hull form and therefore it was always necessary to resort to model tests.

Kaplan [15] has proposed a method for representing nonlinear contributions to the roll damping based on the concept of cross-flow drag. An expression for the nonlinear roll moment due to skegs, bottom and barge sides was derived in which the roll damping was proportional to $|\dot{\theta}|\dot{\theta}$, where $\dot{\theta}$ denotes roll angular velocity. For regular sinusoidal waves this nonlinear damping term B_{NL} is approximated in an equivalent linear form as

$$B_{\mathrm{NL}}|\dot{\theta}|\dot{\theta} = \frac{8}{3\pi} B_{\mathrm{NL}}\theta_{\mathrm{m}}\omega_{\mathrm{n}}\dot{\theta} \tag{2}$$

where ω_{n} is the roll natural frequency and θ_{m} is the roll amplitude.

The nonlinear roll-motion response of ocean-going barges has been thought to be partially due to features other than the viscous phenomena of vortex shedding and skin friction. Denise [16] indicates that linear models are inadequate because ocean-going barges have very shallow draught, of the same order of magnitude as the wave amplitudes considered and hence the basic assumption of small motions required by linear theory is not satisfied. Although a full representation of the additional nonlinear effects is difficult, Denise has developed a method of quantify the additional loads due to nonlinearities that he refers to as buoyancy-restoring forces and moments. These corrections to the linear forces on the barge cause a nonlinear detuning at resonance. The additional forces primarily apply in the region of the vessel splash zone and depend on the wave profile and relative barge motion. Denise's nonlinear model accounts for these effects and the compared his roll-motion estimates with model and full-scale test data and linear potential-flow theory, with and without empirical additions allowing for "viscous roll damping". In general, his resonant roll amplitudes agree closely with measured values, the linear potential-flow theory consistently overpredicting the motions. However, it is noted that Denise has applied the method only to barges having well-rounded keel edges where the effects of vortex shedding would be relatively unimportant. Experimental evidence (see Brown et al. [17]) does suggest that a major part of the viscous force acting on a barge with bluff right-angle keel edges is due to vortex shedding. This work is aimed at quantifying this effect with the aid of the discrete-vortex method.

2.2. Discrete-vortex models

The first representation of a continuous vortex sheet by discrete vortices was provided by Rosenhead [18] who investigated the instability between two adjacent liquid surfaces with velocities equal in magnitude but opposite in direction. The sheet was given an initial sinusoidal disturbance and replaced by twelve elemental vortices uniformly positioned along one wavelength of the sinusoid. Rosenhead's results were calculated manually and only four time steps taken; however, he concluded that the vortex sheet 'rolled up' smoothly into concentrated clusters of vortices.

Rosenhead's conclusions were challenged by Birkhoff and Fisher [19] and Hama and Burke [20] who repeated the original calculations using significantly more vortices per wavelength and smaller time steps. They found that whilst the vortices did form into clusters, their paths were extremely irregular and occasionally crossed, physically impossible for a vortex sheet. It was also agreed that a distribution of point vortices might roll up, but would also, given time, unroll and become random, Rosenhead's results being in error due to the relatively large time steps used in his calculations. Hama and Burke concluded that with smaller time steps and equal strength vortices placed along the sine wave, smooth roll-up could be achieved. Rosenhead's work was extended further by Abernathy and Kronauer [21] who considered the stability of two zero-thickness shear layers a fixed distance apart. They replaced the shear layers with vortex sheets of opposite sign and found that the development and interaction of the two vortex layers led to clusters of positive and negative vorticity arranged in the familiar von Kármán vortex-street pattern.

Even though these early models of vortex motions showed some of the experimentally observed features of a vortex sheet, two important effects were not taken into account. Firstly the sheets analysed were of infinite extent, and therefore boundary conditions on the body which formed the sheets were not included in the calculations. These boundary conditions are satisfied by introducing image vortices in the body that substantially alter the induced velocities of the vortex sheets close to the body. Secondly, the distribution of vorticity in the sheets was taken as constant in time, whereas in reality, vorticity is fed to the sheet from the boundary layers separating from the body.

Following shortly after Rosenhead's pioneering work, Westwater [22] applied a discrete-vortex approximation to the sheet shed from an elliptically-loaded wing. Twenty unevenly-spaced vortices of equal strength were used, and Westwater concluded that the rolling-up process started from the wing tips and took a similar form to the spiral predicted analytically by Kaden [23], even to the extent that Westwater's model indicated "kinks" in the sheet appearing to agree with flow-visualization pictures produced by Kaden. It is debatable whether these early photographs substantiated the existence of such kinks, though the general appearance of Kaden's photographs was similar to Westwater's predictions of the sheet development.

In a similar way to which Rosenhead's model was criticised, Moore [24] repeated Westwater's calculations using many point vortices, much smaller time steps, and 16-figure arithmetic with a fourth-order Runge-Kutta integration scheme. The vortex sheet soon became distorted and chaotic. In an attempt to show whether this "late-time randomness" was due to numerical inaccuracy in the integration method, Moore reversed the vortex development at a particular time instant after the flow had become "random", and found that the chaotic state unscrambled and the vortices returned to their original positions.

In 1973 Clements [25] developed the discrete-vortex method to model vortex shedding behind a square-based block. The proposed model calculated the motions of the shear

layers from the velocities of the discrete vortices which were derived through a Schwartz-Christoffel transformation of the form

$$z = -\frac{2is}{\pi}\left\{\sin^{-1}(\lambda) + \lambda(1-\lambda^2)^{1/2}\right\}, \tag{3}$$

z and λ being complex variables representing the physical and transformed planes, and s the body half-width. Hence the exterior of the body was transformed into an upper half-plane with the boundary along the real axis, the positions of image vortices being found trivially in the λ-plane from the positions of the vortices themselves. The flow around the body was impulsively started from rest and initially developed symmetrically. Vortices were introduced at the separation points $z = \pm is$ with velocity and strength values depending only on the flow velocity at the outer edge of the boundary layer. Clements' model predicted the form of the vortex shedding, the Strouhal number, and some other flow quantities to within reasonable agreement with experimental results. Clements' work was further developed with Maull [26] to utilise a Kutta condition on the flow satisfied in a mean sense at each time step. This implied that there should be no flow at the corners of the block, corresponding to flow-separation points in the transformed plane being stagnation positions.

Both Kuwahara [27] and Sarpkaya [28] have studied vortex shedding from an inclined flat plate under steady flow conditions. In both cases, the vortex-image positions were found by transforming the plate into a circle using the Joukowsky transformation, with a Kutta condition to calculate vortex strengths. The generalised Blasius theorem (see Milne-Thomson [29]) was used to estimate forces on the body. In Kuwahara's method vortices were introduced at fixed points near the edges of the plate and his calculated normal-force coefficients were on average 1.5–2.0 times larger than those obtained experimentally, with sudden increases in amplitude of as much as four times the mean value. A parametric study indicated that the amplitudes of oscillation of the normal-force coefficients were strongly dependent on the assumed point of introduction. The study by Sarpkaya [28]) indicated that the difficulties found by Kuwahara were not due to deficiencies in the method, but the failure to recognise that the point of appearance of the nascent vortices (the ones most recently shed) was of vital importance and controlled the manner in which they rolled up. In Sarpkaya's method the vortex strengths k were calculated from the equation

$$\frac{\partial k}{\partial t} = \tfrac{1}{2} U_{\mathrm{sh}}^2 \tag{4}$$

where U_{sh} was the mean velocity of the four vortices previously input into the flow, and vortex input positions were found from the Kutta condition applied at each time step. Sarpkaya's method predicted the Strouhal number satisfactorily, but obtained normal force values 20% higher than those measured experimentally.

Researchers calculating vortex motions using sheet discretisation of finite extent, or in the presence of a body, concluded that the promising early work of Rosenhead and Westwater appeared to give good results when the representation was carried out using few elemental vortices with large time steps. When the results were recalculated using more vortices and smaller time steps, the vortex sheet developed in a chaotic manner, crossing itself in a physically unrealistic way.

Though this fact was recognised, Fink and Soh [30] were the first investigators to give a reason for the randomness inherent in the method, indicating that it was due to the representation of the growing vortex sheet by an identifiable set of discrete vortices. Fink and Soh demonstrated that the complex-conjugate velocity of a segmented vortex sheet contains a logarithmic term that is not accounted for in a discrete-vortex representation of that sheet. The main consequence of this was that if the equivalent vortex was not placed at the mid-point of its segment at each time interval using some form of sheet rediscretisation, the logarithmic term did not vanish. The computational error would then increase in a way that depended on the nature of the problem, number of vortices in the flow, and total time of computation. They recalculated the results of earlier workers and in all cases obtained smoother roll-up, delaying the chaoticness inherent in the original predictions. Fink and Soh also applied their rediscretisation method to a number of flows past plate-like bodies including cross flow over rectangular sections (similar to barge hulls) and again obtained good roll-up. In their calculations the vortex-separation points were fixed and the method was limited to relatively small time developments.

Most of the research work described so far has been applied to unidirectional flow situations about flat plates or rectangular blocks. Details are now given of work utilizing the discrete-vortex method with body shapes used particularly in the offshore industry, that is, circular and sharp-edged cylinders. The method is adapted to conditions of oscillating fluid flows, these being similar to water-particle motions in waves.

Stansby [31] has developed a discrete-vortex method to calculate results for unidirectional steady and planar oscillatory flows about isolated circular cylinders. Vortices were introduced from fixed positions on a line through the cylinder centre normal to the freestream flow direction. In reality, however, the actual shedding positions are unsteady and Reynolds-number dependent. Stansby's model satisfied the Kutta condition, though it did not encompass the developments of Fink and Soh, and vortex strengths were calculated from an equation similar to that given by (4). The method removed vortices from the flow if they approached too close to the cylinder, and combined them if they came too close to each other. The development was stepped through time using a second-order scheme, and drag and lift forces found from the unsteady Blasius force equation. The drag-force results were in reasonable agreement with those calculated from Morison's equation and experimental data, and the lift coefficients agreed well with experiment for Keulegan-Carpenter number 15. For higher values, the predicted results increasingly overestimated the experimental data.

A method to calculate the unidirectional flow about a circular cylinder has been developed by Sarpkaya and Schoaff [32], their vortex sheets being rediscretised at each time step to improve roll-up, as in Fink and Soh's original method. The vortex-introduction points were found from evaluation of the boundary layer about the cylinder at each time step using the unsteady momentum equation. The vortex strengths were calculated with an equation similar to (4), using the velocity in the freestream flow radially outward from the separation point. A first-order time-stepping scheme was used, drag and lift coefficients were found from the Blasius equation, and an estimate was made of the flow Strouhal number, the values agreeing reasonably with experimental data.

Recently, Efthymiou and Narayanan [33] developed a discrete-vortex model to simulate steady flow about submarine pipelines near the sea bed. Three options were used to determine the angular position of the separation points around the cylinder. The choice was either based on experimental evidence or on the data of other researchers or calculated as the position of maximum velocity on the cylinder surface. The vortex

strengths were estimated in the conventional manner and forces on the pipeline found from use of both the Blasius equation and an explicit integration of Bernoulli's equation around the body surface. Efthymiou and Narayanan did not rediscretise the vortex sheet but obtained numerical estimates of the drag forces (for cylinders remote from the sea bed) and lift forces in reasonable agreement with experimental data, and Strouhal numbers of about 10% less than the experimental values for the flow when alternate vortex shedding was possible. Although the model produced acceptable results, force values tended to fluctuate, exceeding the experimental data by at least a factor of two, possibly due to the three-dimensional nature of the real wake.

An interesting application of the vortex method is by Longuet-Higgins [34] who considered oscillating flow over steep sand ripples. The method employed a transformation of the fluid onto the exterior of a polygon and thence the interior of a circle, to obtain the vortex-image positions. Vortices were input into the flow near the crest of each ripple, and the effective vortex drag found from momentum considerations and checked using the Blasius equation. The method yielded force coefficients in good agreement with experimental data.

The analysis of flows around bodies in planar oscillatory flow has also been carried out. Bearman et al. [35] calculated the flow around a two-dimensional flat plate in a transformed circle plane. The effect of the Keulegan-Carpenter number on the different vortex-shedding patterns was determined and results compared with experimental data produced in a U-tube water tank. In general, predicted force measurements and flow patterns were similar to measured values. Graham [36] has developed a discrete-vortex model to analyse the forces induced by separation from sharp-edged bodies of general internal angle, valid for small oscillations of the fluid. The Kutta condition for the flow was satisfied, and the forces calculated by considering the rate of change of momentum across a circuit at infinity, and, as a check, from direct use of the unsteady Blasius equation. The method has been applied to a single shedding edge and has been extended to model vortices shed in the vicinity of a rolling barge keel (see Bearman et al. [37]), by matching the two flows using an appropriate length scale.

Faltinsen and Pettersen [38] have recently outlined a general method to predict the flow and associated vortex shedding around bluff bodies at high Reynolds numbers. Their method is useful, as it can be applied to various body shapes, the solution for the velocity potential over the body and free shear layers being represented by a distribution of sources and dipoles. Earlier workers have mostly employed transformation methods to map the body shape onto a circle, half-plane or rectangle, and used the method of images to satisfy the condition of zero flow through the boundary, with the limitation of only being able to deal with relatively simple and usually isolated bodies. Faltinsen and Petterson rediscretise the free shear layers at each time step, their force results for steady cross flow past a flat plate being in good agreement with those from Fink and Soh's calculations. The method has been used to calculate results for oscillatory cross flow past the plate, and initial predictions indicate flow development similar to that found from visualization studies.

The above review demonstrates how the discrete-vortex method has been applied in the last decade to unidirectional and oscillatory flows around various bodies. The theoretical work and comparison with test data presented in this paper aim to develop this application for the specific case of the effects of vortex shedding from the keels of a shallow-draught, flat-bottomed barge.

3. Theoretical development of vortex-shedding method

A theoretical model of the inviscid flow below a square-based rectangular block representing a rolling barge of large beam in cross section is developed, the free shear layers emanating from the sharp corners being represented by discrete vortices placed in the flow at suitable positions. The model is stepped through time and the motions of the vortex sheets and resultant body loads are calculated. Two-dimensional flow is assumed, with no interaction allowed between vortices shed from the two independent corners as it is felt that in reality, vortices travelling under the keel of the vessel would decay through viscous action before moving significant distances from the shedding edge. Hence the flow structure about a single corner is developed, loads being appropriately summed to allow for shedding from both edges, as discussed later.

The method of images is employed to ensure no fluid flow through the body walls. These images positions are found trivially for the barge by using a Schwartz-Christoffel transformation to project the exterior of the body onto an upper half plane, with the body boundary along the real axis. The image positions in the transformed plane are thus defined by complex-conjugate values of the actual vortex positions. The transformation is similar to that of Clements [25], taking points from the physical (z) plane to the transformed (λ) plane, and is of the form

$$z = -\frac{2s}{\pi}\left\{\sin^{-1}(\lambda) + \lambda(1-\lambda^2)^{1/2}\right\} \tag{5}$$

where

$$\sin^{-1}(\lambda) = -\mathrm{i}\log\left\{i\lambda + (1-\lambda^2)^{1/2}\right\}. \tag{6}$$

The corners of the body $z = \pm s$ transform into the points $\lambda = \mp 1$ as indicated by Figure 1, the body sides extending upwards to infinity in the physical plane.

At each time step, a point vortex is introduced into the flow close to the barge corner $\lambda = -1 + 0\mathrm{i}$ in the transformed plane. This vortex subsequently moves under the influence of a sinusoidally-varying localised base flow, its motion being affected by the positions and strengths of other vortices and images in the flow. The irrotational base flow is used to represent the rolling motion of the barge. It is assumed that the barge boundary is stationary, and the base flow oscillates about the body with the same roll frequency and

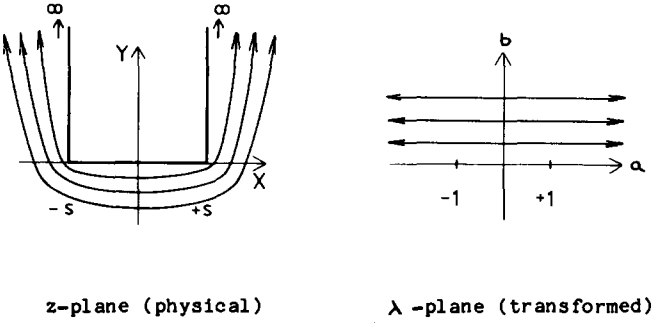

Figure 1. Arrangement of axes and base flow.

amplitude as that of the barge responding near roll resonance. This representation is valid because wave velocities must be locally tangential at the barge hull and oscillating at the wave frequency. Also, at roll resonance, large roll angles occur in a wave flow of small amplitude, lending further evidence to the validity of the assumption that the relatively small water-particle velocities due to the wave can be represented within the base flow described above.

It is assumed that initially the base flow is motionless, and subsequently moves below the barge in the negative x direction. This corresponds to the vessel having maximum angular displacement θ_m from equilibrium, the instantaneous roll angle measured anti-clockwise being given by $\theta = -\theta_m$. Boundary conditions on the base flow for roll at frequency ω are thus given by

$$|\boldsymbol{u}| \to 0 \quad \text{as} \quad |z| \to \infty \tag{7}$$

and

$$\boldsymbol{u} = (U_m \sin \omega t, 0) \quad \text{at} \quad z = 0. \tag{8}$$

where $\boldsymbol{u}$ is the velocity of the base flow and U_m is a constant. The constant U_m is found to be

$$U_m = -\theta_m \omega r \tag{9}$$

where r denotes the perpendicular distance from the barge roll centre (assumed to be on the line $x = 0$) to the vessel base. Equations (8) and (9) are a valid representation of base flow motion in the region of the barge keel edges for roll centres that lie above the barge keel ($r > 0$). Results of experiments performed by Brown et al. [17] on rolling barges having sharp and rounded keel edges to promote and suppress vortex shedding indicate that the roll centres for such vessels lie above keel (by as much as four times the vessel draught) throughout the complete roll cycle.

From the theory of complex variables, the complex velocity of the base flow at $z = 0$ is given by

$$\frac{dw_1}{dz} = -\theta_m \omega r \sin \omega t = \frac{dw_1}{d\lambda}\frac{d\lambda}{dz} \tag{10}$$

where w_1 is the complex potential of the base flow and $d\lambda/dz$ found from (5) is given by

$$\frac{d\lambda}{dz} = -\frac{\pi}{4s}\frac{1}{(1-\lambda^2)^{1/2}} = -\frac{\pi}{4s} \quad \text{at} \quad z = 0. \tag{11}$$

Hence the condition given by (8) reduces to requiring that

$$\frac{dw_1}{d\lambda} = \frac{4s}{\pi}\theta_m \omega r \sin \omega t \tag{12}$$

at $\lambda = 0$. This is satisfied by taking the base-flow complex potential as

$$w_1(\lambda) = \frac{4s}{\pi}\lambda \theta_m \omega r \sin \omega t, \tag{13}$$

giving the complex velocity as

$$\frac{dw_1}{dz} = -\frac{\pi}{4s}\frac{1}{(1-\lambda^2)^{1/2}}\left\{\frac{4s}{\pi}\theta_m \omega r \sin \omega t\right\}, \tag{14}$$

which satisfies (7) as $|\lambda| \to \infty$ and $|z| \to \infty$.

The flow field due to vortices is found in the physical plane using the fact that the potential due to each point vortex transforms into that due to a vortex of equal stength at the transform of the vortex position. Hence if the complex potential at any point λ (apart from a vortex position) is given by w_2, then for m vortices in the flow

$$w_2(z) = w_2(\lambda) = -\frac{i}{2\pi}\sum_{j=1}^{m}\left\{k_j \log(\lambda - \lambda_j) - k_j \log(\lambda - \bar{\lambda}_j)\right\} \tag{15}$$

where λ_j, $\bar{\lambda}_j$ are positions of the jth vortex and its image respectively, k_j being their strengths. The complex potential for the complete flow is thus given by summing (13) and (15) and the complex velocity is found from

$$\frac{dw}{dz} = \frac{dw}{d\lambda}\frac{d\lambda}{dz}, \tag{16}$$

where $dw/d\lambda$ is obtained by differentiation as

$$\frac{dw}{d\lambda} = \frac{4s}{\pi}\theta_m \omega r \sin \omega t - \frac{i}{2\pi}\sum_{j=1}^{m}\left\{\frac{k_j}{\lambda - \lambda_j} - \frac{k_j}{\lambda - \bar{\lambda}_j}\right\} \tag{17}$$

and $d\lambda/dz$ is given by (11).

If the point whose velocity is required is also a vortex position, return to the z plane is complicated by Routh's rule (see Clements [25]), giving

$$w_a - \frac{ik_p}{2\pi}\log(z - z_p) = w_b - \frac{ik_p}{2\pi}\log(\lambda - \lambda_p). \tag{18}$$

where w_a and w_b are the complex potentials at z_p and λ_p respectively, due to all causes except the vortex of strength k_p at z_p. This eventually gives

$$\left.\frac{dw_a}{dz}\right|_{z_p} = \left.\frac{dw}{d\lambda}\right|_{\lambda_p}\left.\frac{d\lambda}{dz}\right|_{z_p} - \frac{ik_p}{2\pi}\frac{f''(z_p)}{2f'(z_p)} \tag{19}$$

and in a similar manner to (17) the term $dw/d\lambda$ at λ_p is given by

$$\left.\frac{dw}{d\lambda}\right|_{\lambda_p} = \frac{4s}{\pi}\theta_m \omega r \sin \omega t - \frac{i}{2\pi}\left\{\sum_{\substack{j=1 \\ j\neq p}}^{m}\frac{k_j}{\lambda_p - \lambda_j} - \sum_{j=1}^{m}\frac{k_j}{\lambda_p - \bar{\lambda}_j}\right\} \tag{20}$$

and $f''(z_p)$ found from differentiation of (11). Therefore, using (16) or (19), the complex velocity is determined at all points in the flow field in the physical plane, the complex potential being found everywhere except at vortex positions from (13) and (15).

The vortex sheet is developed by stepping the method through time using Eulerian first- or second-order schemes. For the pth vortex, positions at time $t+\Delta t$ are found from those at time t by using

$$\lambda_p(t+\Delta t)=\lambda_p(t)+\frac{\mathrm{d}\lambda_p(t)}{\mathrm{d}t}\Delta t \tag{21}$$

or

$$\lambda_p(t+\Delta t)=\lambda_p(t)+\frac{1}{2}\left\{3\frac{\mathrm{d}\lambda_p(t)}{\mathrm{d}t}-\frac{\mathrm{d}\lambda_p(t-\Delta t)}{\mathrm{d}t}\right\}\Delta t. \tag{22}$$

The first scheme has an error in any time step t of $O(\Delta t^2)$, and is used for initial advancement of a newly-created vortex. The second has an error of $O(\Delta t^3)$, and calculates new positions of vortices that existed over at least the previous time step. The term $\mathrm{d}\lambda/\mathrm{d}t$ at λ_p is found from the equation of motion in the physical plane given by

$$\frac{\mathrm{d}z_p}{\mathrm{d}t}=\left(\frac{\mathrm{d}w_p}{\mathrm{d}z}\right)^* \tag{23}$$

where * represents a complex-conjugate quantity, and $\mathrm{d}w_p/\mathrm{d}z$ is given by (19). The velocity in the transformed plane is thus given by

$$\frac{\mathrm{d}\lambda_p}{\mathrm{d}t}=\left(\frac{\mathrm{d}w_p}{\mathrm{d}z}\right)^*\frac{\mathrm{d}\lambda}{\mathrm{d}z}. \tag{24}$$

The strengths of vortices being input into the flow field are found by taking the rate of shedding of vorticity into the wake given by

$$\frac{\partial k}{\partial t}=\int_0^{\delta'}\left(\frac{\partial v}{\partial x}-\frac{\partial u}{\partial y}\right)u\,\mathrm{d}y, \tag{25}$$

where δ' is the boundary-layer thickness, and u and v represent the tangential and normal velocity respectively. In the present method vortices are introduced at each time step and therefore (25) is approximated by

$$k_{\mathrm{NA}}=\frac{1}{2}\left(\frac{\mathrm{d}w}{\mathrm{d}z}(\lambda_{\mathrm{NA}})\right)\left(\frac{\mathrm{d}w}{\mathrm{d}z}(\lambda_{\mathrm{NA}})\right)^*\Delta t, \tag{26}$$

where k_{NA} and λ_{NA} are the strength and transformed position of the nascent vortex, which is assumed to be at the outer edge of the boundary layer, and $\mathrm{d}w/\mathrm{d}z$ is found from (16).

The determination of nascent-vortex positions is simplified in this study by the fact that the flow-separation points $z=\pm s$ are fixed at the sharp-edge corners of the body. However, the present method does have the slight disadvantage that these separation points are singularities of the transformation, their effect being to cause infinite velocities at the corners as indicated by (16). In practice though, the flow separates smoothly and tangentially at the barge keel edges, and this may be represented formally by a Kutta

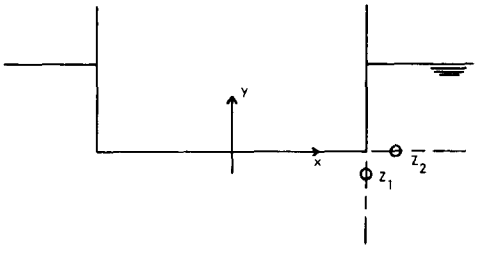

Figure 2. Nascent-vortex positions.

condition (see Pope [39]) on the flow at each time step, requiring that $dw/d\lambda$ is zero at positions $\lambda = \pm 1 + 0i$, the term dw/dz therefore giving a finite velocity at the body corners. This condition may either be satisfied by assuming that at each time step the nascent-vortex position is known, and hence calculating its stength, or by prescribing its strength and using the condition to ascertain the input position. In the present analysis values were found by using both of these forms of the Kutta condition, but they gave unacceptably large changes in nascent-vortex strength over adjacent time steps, or predictions of vortex motions at physically unrealistic angles to the base flow. The conclusions are similar to findings of Clements' early work [25]. For simplicity and because of these problems, vortices are introduced into the flow at a fixed small distance from the shedding corner. The chosen position is either vertically below the corner $z = +s$ for base flow in the clockwise direction, or directly to one side of it after base-flow reversal, as indicated by points Z_1 and Z_2 in Figure 2.

Other relevant features of the mathematical model include its ability to inhibit vortices from approaching too close to the barge boundary, otherwise causing them to have unduly high velocities owing to the presence of their images in the lower half of the transformed plane. In the computer program implementing the method, vortices are not allowed to approach closer than 10% of their distance from the boundary when created. The method also inhibits creation of vortices with strengths below a certain minimum value, thus reducing the number of point vortices in the flow and hence computation time. In the figures depicting the flow development of the vortices it is necessary to indicate the positions and strengths of point vortices in a simple but representative way. Hence each vortex is depicted as a small semi-circle, with radius proportional to the square root of the corresponding vortex strength (as Longuet-Higgins [34]). The strengths are thus proportional to the areas of the corresponding circles, negative and positive vorticity being represented by semi-circles having gaps on their right and left sides respectively.

Once positions and velocities of the point vortices have been identified, the pressures induced on submerged faces of the barge and the loads on the vessel are evaluated. Loads on the submerged corner are calculated both by a conventional integration of pressures about the corner and by using the Blasius equation (see Milne-Thomson [29]). The second technique is computationally more efficient than the first and has fewer mathematical parameters, but it can only be used to calculate the quadratic term in the pressure equation (31), the method not being able to estimate the time-varying term in this particular application. A comparison of results calculated from each method is presented later.

Pressure integration on submerged faces of the vessel is performed by dividing the faces up into small elements or nodes. The local velocity and rate of change of velocity potential

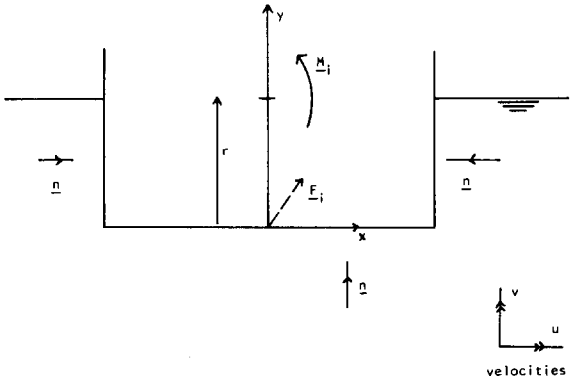

Figure 3. Axes conventions for vortex-induced forces and moments.

are calculated for each element, and the pressure found (per unit length of barge) by using Bernoulli's equation. The element pressures are summed in the appropriate way to give induced moments on the vessel.

Taking the force convention defined in Figure 3, with unit normal $\boldsymbol{n}$ into the body, the force on the stationary floating vessel due to the time-dependent flow may be written as

$$\boldsymbol{F}_i = \int_S p\boldsymbol{n}\,\mathrm{d}S \tag{27}$$

where integration is performed over the submerged barge surface S, and subscript i denotes that loads are calculated from an integration of pressure, p. In a similar way the induced moment $\boldsymbol{M}_i$ on the vessel is defined as

$$\boldsymbol{M}_i = \int_S p(\boldsymbol{r}_a \times \boldsymbol{n})\,\mathrm{d}S \tag{28}$$

where $\boldsymbol{r}_a$ is the radius arm from the roll centre to the point (x, y) on the barge surface. The pressure p is given by Bernoulli's equation as

$$p = -\rho\left\{\tfrac{1}{2}(u^2 + v^2) + \frac{\partial\phi}{\partial t}\right\}, \tag{29}$$

(u, v) and ϕ being the velocity and potential at the point (x, y). For brevity the two terms in Bernoulli's equation are subsequently referred to as the (v) and (ϕ) terms respectively. The induced moment (scalar value) may thus be written as the sum of individual moments due to these two terms, giving

$$M_i = M_i(v) + M_i(\phi). \tag{30}$$

As pressure at each node is found due to all elemental vortices and at every time step, it is necessary to calculate the terms ϕ, u, and v in (29) in an efficient manner. The complex potential at a point $\lambda(a, b)$ is given by

$$w(\lambda) = \phi + \mathrm{i}\psi, \tag{31}$$

ψ being the stream function at the point $\lambda(a, b)$. Hence, using (13) and (15), potential at a general point $(a, 0)$ on the transformed body boundary can be written as

$$\phi(a) = \mathrm{Re}\{w(\lambda)\}$$

$$= \frac{4s}{\pi} a\theta_m \omega r \sin \omega t + \sum_{j=1}^{m} k_j \tan^{-1}\left(\frac{-2b_j(a-a_j)}{(a-a_j)^2 - b_j^2}\right) \tag{32}$$

where (a_j, b_j) and k_j are the position and strength of the jth vortex in the λ plane. However, the complex potential is invariant, and so (32) also provides the value of ϕ at a general point (x, y) on the vessel boundary. To calculate $\partial\phi/\partial t$, the first term in (32) is ignored, as this only involves the base-flow representation with no effects of vortex shedding appearing. The second term alone is found for each of the j vortices, the method stepped forward through time Δt, and potential calculated at the same point again.

The (v) term in Bernoulli's equation is calculated efficiently using the complex velocity given by (16), as $\mathrm{d}w/\mathrm{d}\lambda$ at the point $(a, 0)$ on the transformed-plane boundary can be simplified as

$$\frac{\mathrm{d}w}{\mathrm{d}\lambda}(a) = \frac{4s}{\pi}\theta_m \omega r \sin \omega t + \frac{1}{\pi}\sum_{j=1}^{m} \frac{k_j b_j}{(a-a_j)^2 + b_j^2}. \tag{33}$$

Hence

$$\left(\frac{\mathrm{d}w}{\mathrm{d}z}\right)\left(\frac{\mathrm{d}w}{\mathrm{d}z}\right)^* = \left|\frac{\mathrm{d}w}{\mathrm{d}\lambda}\right|^2 \left|\frac{\mathrm{d}\lambda}{\mathrm{d}z}\right|^2$$

$$= \left[\frac{4s}{\pi}\theta_m \omega r \sin \omega t + \frac{1}{\pi}\sum_{j=1}^{m} \frac{k_j b_j}{(a-a_j)^2 + b_j^2}\right]^2 \left\{\frac{\pi^2}{16s^2(1-a^2)}\right\}$$

$$= \{A + B\}^2 \left\{\frac{\pi^2}{16s^2(1-a^2)}\right\}, \tag{34}$$

say, where A and B are the two terms within the square brackets. However, the additional velocities induced due to vortex shedding alone are again required, and so the base-flow contribution is ignored giving

$$(u^2 + v^2)_{x,y} = \frac{\pi^2}{16s^2(1-a^2)}(B^2 + 2AB). \tag{35}$$

The induced moment M_i is thus obtained by multiplying these pressures by the nodal areas and moment arms associated with each element, and summing over all elements using (28).

The alternative calculation of vortex-induced moment using the Blasius method is now described. The moment M_B exerted on a stationary body by a time-dependent flow represented by the complex potential w may also calculated from the generalised unsteady

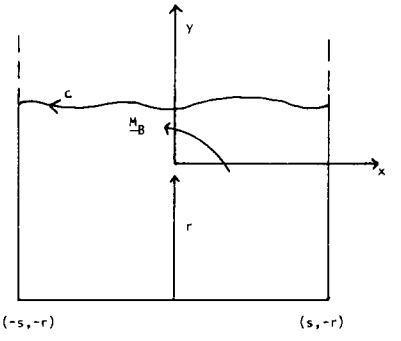

Figure 4. Contour integration in the Blasius method.

Blasius theorem as

$$M_B + iN_B = -\frac{\rho}{2}\int_C z\left(\frac{dw}{dz}\right)^2 dz - \rho\int_C \frac{\partial}{\partial t}(z\bar{w})d\bar{z} \tag{36}$$

where N is the imaginary part of the integral having no physical significance, and C a contour taken anti-clockwise around the body boundary as shown in Figure 4. It is convenient to write (36) in two parts as

$$M_B + iN_B = \{M_B(v) + iN_B(v)\} + \{M_B(\phi) + iN_B(\phi)\} \tag{37}$$

where

$$M_B(v) + iN_B(v) = -\frac{\rho}{2}\int_C z\left(\frac{dw}{d\lambda}\right)^2 \frac{d\lambda}{dz} d\lambda. \tag{38}$$

The transformation from the physical to the transformed plane is here given by

$$z = -\frac{2s}{\pi}\left\{\sin^{-1}(\lambda) + \lambda(1-\lambda^2)^{1/2} + \frac{\pi i r}{s}\right\}, \tag{39}$$

the origin being positioned at the roll centre, a distance r from that defined previously. This change is carried out to simplify the algebra necessary to evaluate (38).

In the analysis, contour C is completed at a finite distance from the corners of the body $z = \pm s - ir$, to avoid the singularity of the integrand at infinity in (38), where $d\lambda/dz = O(1/\lambda)$ as $\lambda \to \infty$. In practice this contour may be reduced or enlarged to any extent, provided that it does not pass over any singularities of the integrand, such as those occurring when the fluid contains sources or vortices.

Contour integration is used to solve (38), the only contributions arising from the residues at simple poles inside the contour. After much algebra the real part of (38) reduces to

$$M_B(v) = \rho \sum_{p=1}^{m} \{k_p(x_p u_p + (y_p - r)v_p)\} \tag{40}$$

where (x_p, y_p) and k_p are the coordinate and strength of the pth vortex having velocity (u_p, v_p) and the origin is taken at the barge base as in the original transformation given by (5).

The second term of (36) representing the contribution to the moment from the (ϕ) component of Bernoulli's equation is not solvable using complex-variable theory. The term $z\overline{w}\mathrm{d}\bar{z}$ is not holomorphic within the contour C, due to the combinations of z and $\bar{z}$ in the expression, and therefore the integral cannot be expressed in the form $f(z_1, z_2, \ldots, z_n)$, independent of the shape of the profile (see Landweber and Yih [40]). No direct check of the (ϕ) term contribution to the moment on the vessel can therefore be made.

Once the induced moment on the corner $z = +s$ has been calculated for a vessel of unit length it is combined with that induced on the second barge corner $z = -s$ to give the moment on the complete vessel.

The single-corner vortex-shedding model is run twice for 1.5 cycles of motion with initial barge-roll motion in first the positive and then negative directions. During the first half-cycle, corresponding to $t/T_{pe} < 0.5$ where T_{pe} is the period of base-flow motion, a vortex array is shed off either the keel base or side close to the vessel corner, as shown in Figure 5a. After flow reversal corresponding to $0.5 < t/T_{pe} < 0.1$, the previously-shed vortex is swept around the corner, and a vortex of opposite sign is created on the second face, as in Figure 5b. Vortex motions continue in a similar way over later cycles and as indicated in Figures 5b and 5d vortex positions are repeatable over each cycle for $t/T_{pe} > 0.5$. It is considered that this assumption is valid as the analysis and flow-visualisation studies indicate that vortices are rapidly convected away from the keels once they are fully formed. The method demonstrates that the dominant force-generating mechanism is due to the growth of vortices close to the corner and the subsequent motion of the

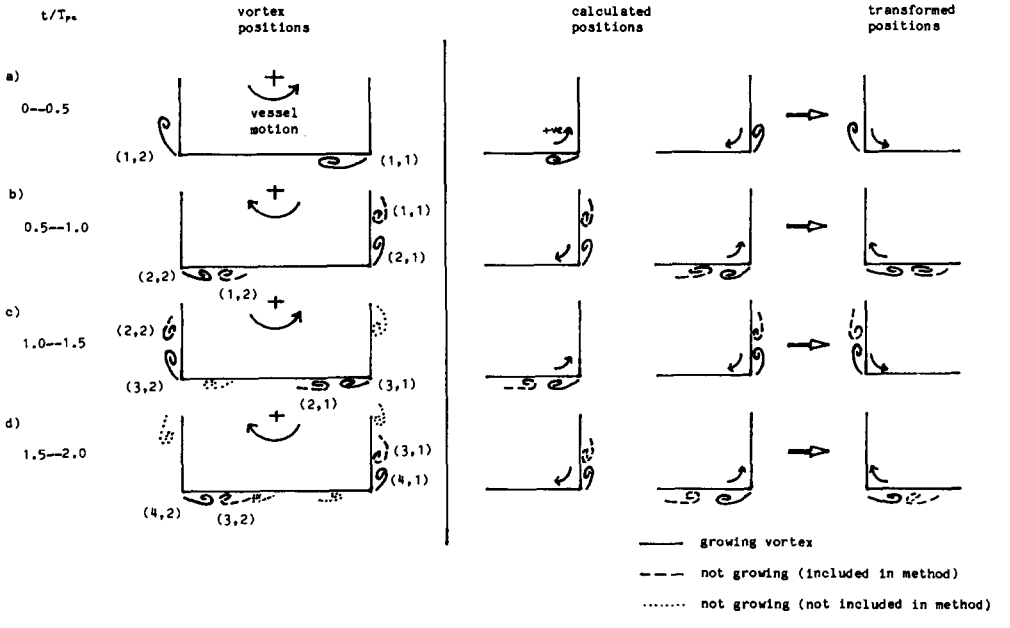

Figure 5. Motions of vortices shed from both barge corners over the first two cycles of vessel roll motion.

vortices in the region of that corner. Furthermore, the moment arm from the point of application of the vortex force to the roll centre is largest close to the corner indicating that the bigger contribution to the vortex-roll moment arises from the motions of vortices during the relatively short time that they are close to the corners. This local creation and motion is almost identical in form after the first cycle of motion as indicated in Figure 5 providing justification that the results for only 1.5 cycles can be used since the local flow is fully developed in the region of the corner by this time. In reality the influence of vortices shed during previous half-cycles would be less than that in the analysis since no representation of decay through viscous action is included. Effects of the free surface are also ignored, because as stated the major contributions to the vortex moments are due to the vortex creation and motion close to the corners.

Vortex strengths and positions calculated from the run with initially-negative barge-roll velocity, corresponding to clockwise vessel-roll motion, are converted to equivalent values as if shed from the second corner $z = -s$, giving vortices (1, 2), (2, 2), etc. The conversion process reverses the sign of vortex strengths and x coordinate of their positions, this procedure being carried out in the transformed plane. Moments on this corner due to these vortices are then added to the values obtained from the original single-corner model with initially-positive roll motion (vortices (1, 1), (2, 1), etc.), to give the induced moment on unit length of the complete vessel. It is noted that symmetry conditions on the two corners do not apply for a barge rolling freely in waves. However, it is felt that the local flow conditions near to the barge corners are similar and therefore vortex shedding off both barge corners is taken to be identical as a simplification.

Once the moment on a vessel of unit length has been determined it is multiplied by the vessel length to convert it into a value applicable to an actual barge. To do this, assumptions are made that end effects are small, and that shear layers are completely two-dimensional. In practice, however, vortex filaments exhibit both chordwise and spanwise variations, these three-dimensional effects playing a major role in the redistribution of vorticity in all directions. For example, Stansby [41] suggests that vortex shedding from circular cylinders occurs in a cell-like manner, individual cells being approximately three cylinder diameters long. Due to the length of most test sections, corresponding to the barge length in the present analysis, the spanwise correlation is destroyed because cells do not shed in phase. Hence it is usually found that experimentally-measured force fluctuations are smaller than those predicted by a discrete-vortex model. However, in the present application, typical barge-length-to-beam ratios are of the order of three and therefore spanwise correlation is likely to be maintained.

Prior to using the discrete-vortex model for force calculations, systematic parametric variations were performed to determine the effects of changes in pressure-integration element size, nascent-vortex input position and method time step. These tests indicated that reliable results were obtained for pressure-integration element size of under 5% of the vessel draught. In the same manner the nascent-vortex insertion position was determined to be a distance of from 3% to 5% of draught from the vessel corner for good roll-up characteristics and smooth vortex-induced force curves. A time step of 1.5% of the barge roll period was chosen as being the best compromise between accuracy and computational efficiency.

Induced-moment results from the (v) term in Bernoulli's equation as calculated by the integrating pressure and Blasius method are presented in Figure 6. The results agree closely during the development of the first vortex array ($t/T_{pe} < 0.50$). Over the time interval soon after flow reversal ($0.58 < t/T_{pe} < 0.70$) agreement is still reasonable, dis-

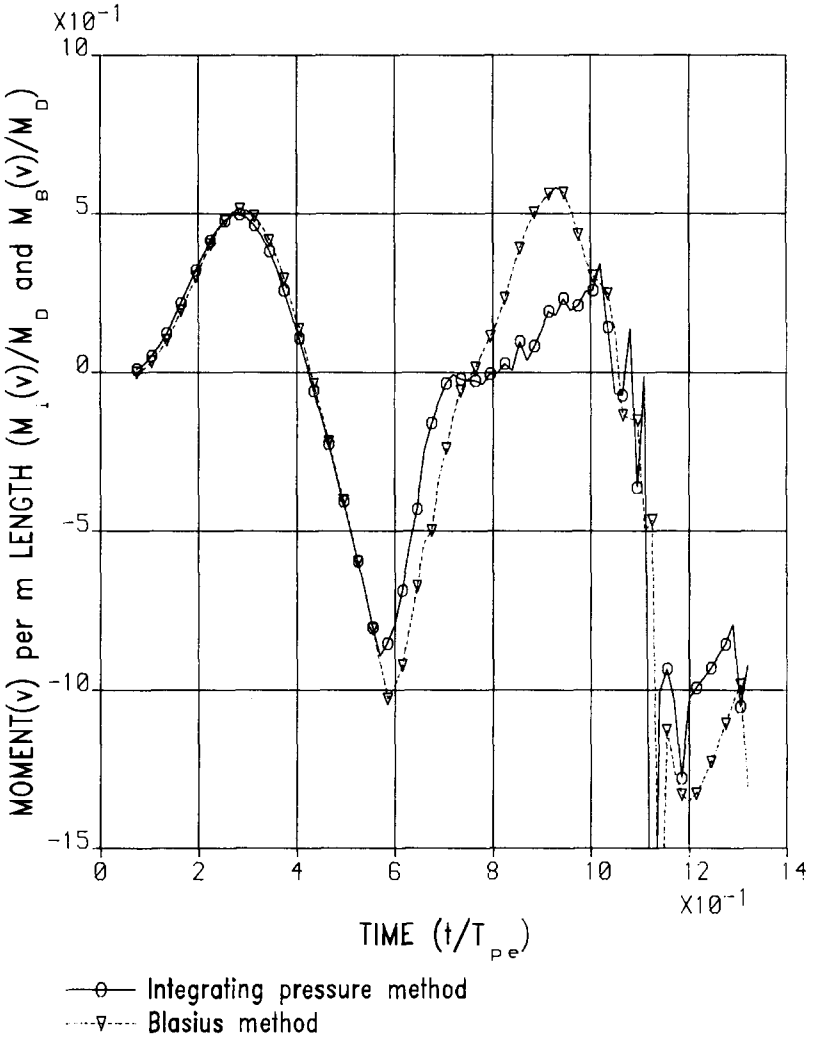

Figure 6. Vortex-induced corner moment (v term) calculated by integration of pressure and Blasius equation.

crepancies being explained by a single point vortex moving a significant distance from the shedding corner, because of its interaction with other vortices in close proximity to it. It is noted that the presented moment values have been nondimensionalised by M_D where

$$M_D = \tfrac{1}{2}\rho U_m^2 s. \tag{41}$$

At later times, differences in moment values predicted by the two methods are caused by higher-strength vortices produced after base-flow reversal. These vortices have a tendency to reduce roll-up of the second vortex array compared to the first. This introduces randomness into the flow, again causing vortices to move relatively large distances from the shedding edge due to the mathematical formulation. However, even at this stage in the flow development both methods predict moment values having the same trends.

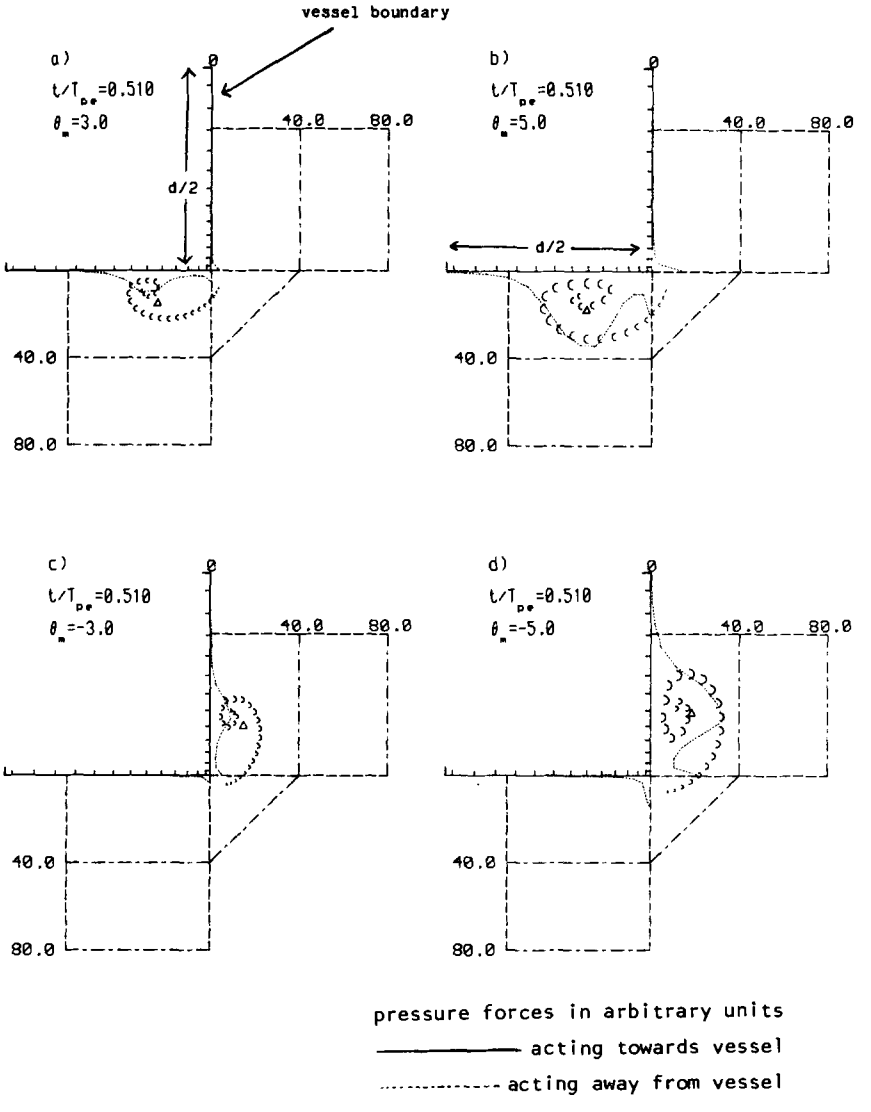

Figure 7. Vortex motions and induced pressure forces at time $t/T_{pc} = 0.51$, with different vessel-roll amplitudes (θ_m) and initially positive or negative roll velocity.

Figures 7, 8 and 9 demonstrate the vortex formation, roll-up and interaction for three different time instants. The effects of both initially positive and negative roll velocity are plotted. The vortex movements and the slightly chaotic behaviour at later times are clearly shown up in these figures.

Finally, in order to apply the discrete-vortex model to predict forces on a rolling barge the effects of barge roll amplitude, θ_m and roll centre need to be quantified. The roll centre is defined by r/d where r is measured upwards from the vessel keel and d the vessel draught.

Variation of induced moment with time for a range of θ_m and r/d values are

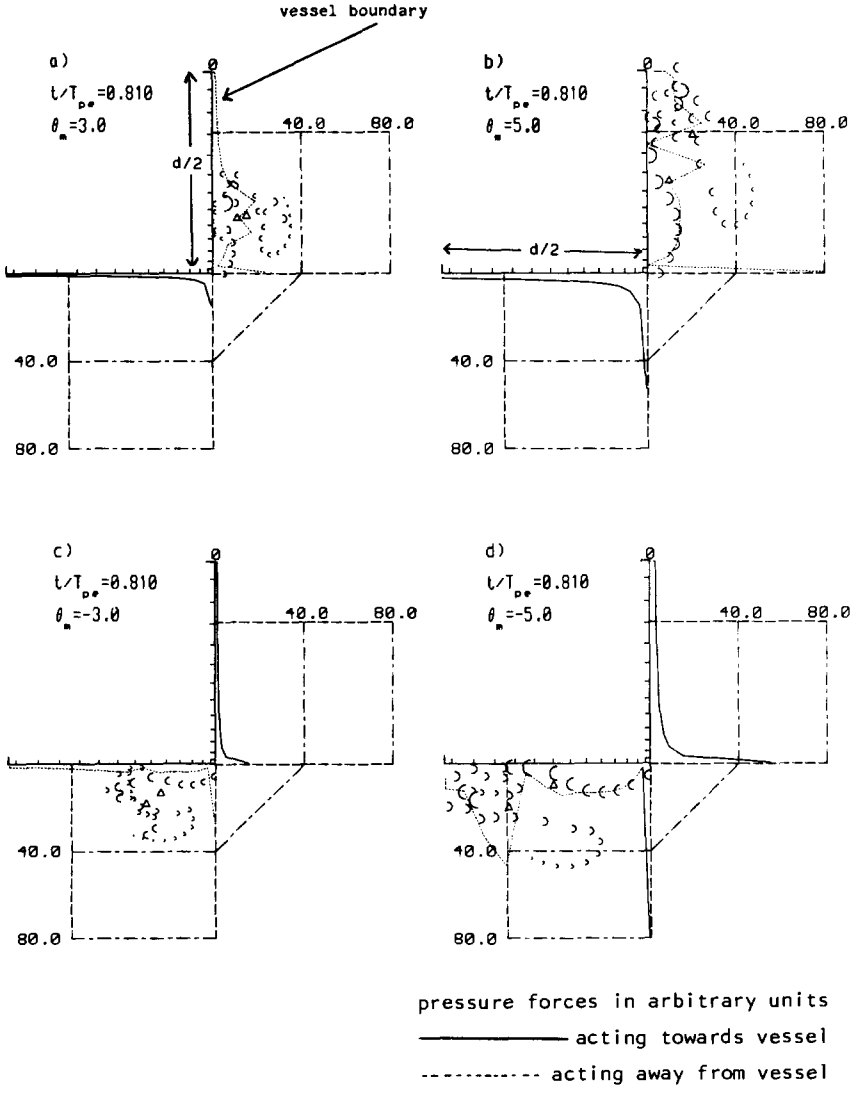

Figure 8. Vortex motions and induced pressure forces at time $t/T_{pe} = 0.81$, with different vessel-roll amplitudes (θ_m) and initially positive or negative roll velocity.

calculated with suitable allowance being made for vortex shedding from both keel edges. The results indicate that induced moment is of the same frequency as barge roll and opposes the roll motion. Figure 10 presents typical induced-moment results for variations in roll amplitude θ_m. The functional dependence of M_{vs}, the vortex-shedding-induced roll moment, can be written as

$$M_{vs} = -f_1(\theta_m) f_2(r/d)\, e^{i(\omega t + \alpha)} \tag{42}$$

where α is the phase of the induced moment relative to the wave. Functions f_1 and f_2, are

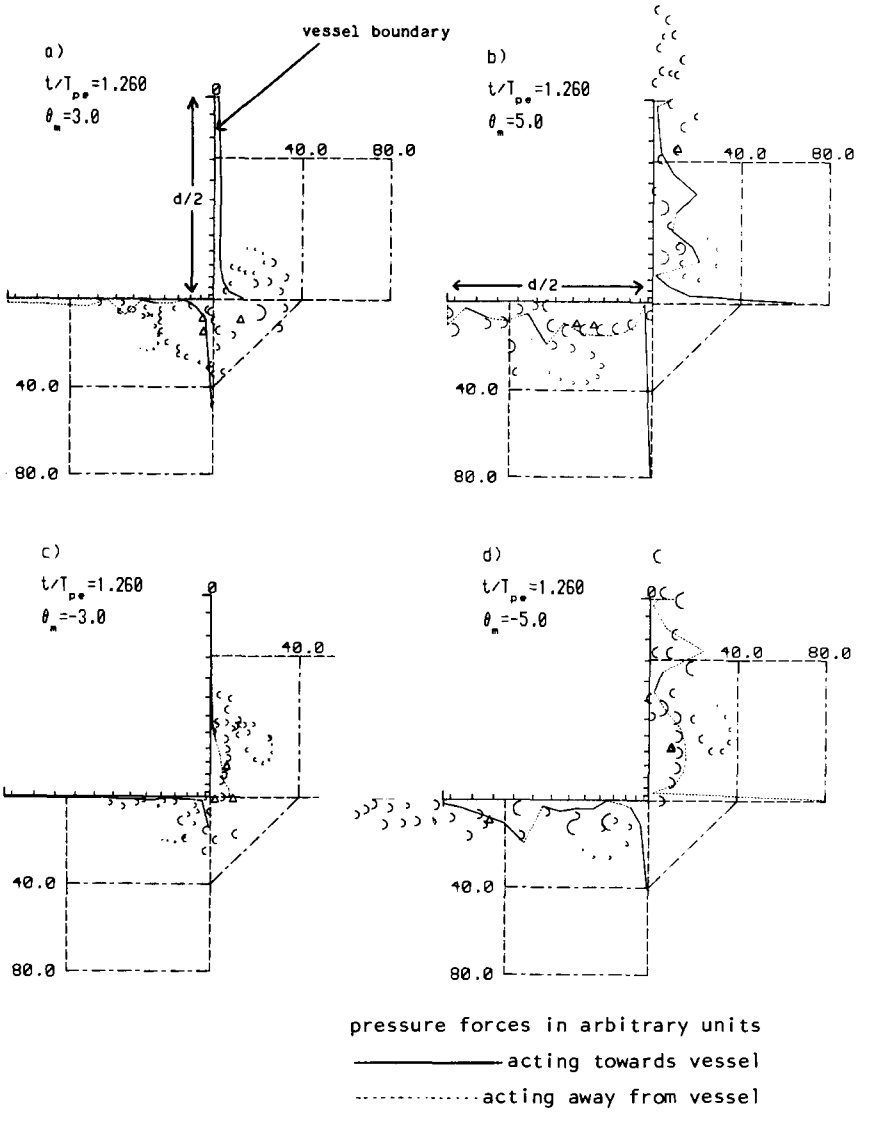

Figure 9. Vortex motions and induced pressure forces at time $t/T_{pe} = 1.26$, with different vessel-roll amplitudes (θ_m) and initially positive or negative roll velocity.

found by curve fitting to be

$$f_1(\theta_m) = 504.9\theta_m^2 - 37.03\theta_m + 0.8767 \tag{43}$$

where θ_m is in radians and

$$f_2(r/d) = 0.8767(r/d)^3 - 1.501(r/d)^2 + 1.299(r/d) - 0.3474. \tag{44}$$

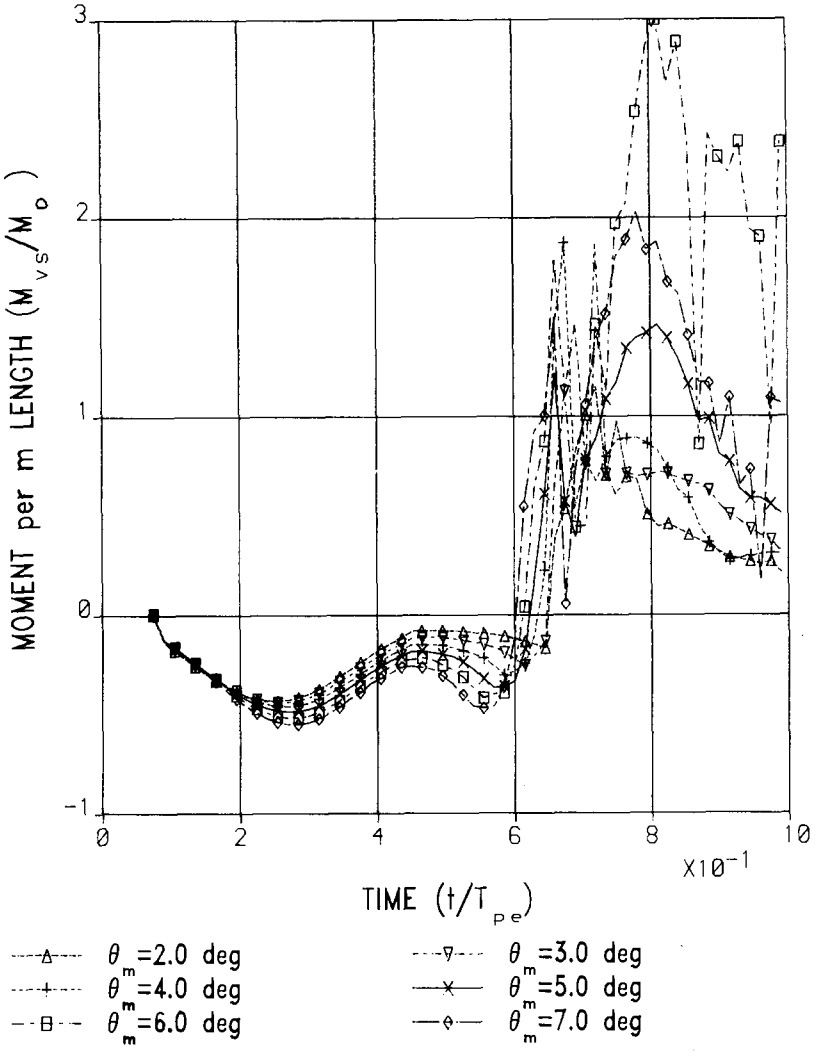

Figure 10. Vortex-induced moment on vessel over first motion cycle for variations in roll amplitude (θ_m).

These functions are plotted in Figures 11 and 12 and used to compare theory and test data in the following section.

It is noted that the motivation for developing the discrete-vortex method has been to permit the effects of such vortex flows to be incorporated into wave-induced roll-motion calculations for marine vehicles. These potential-flow calculations are invariably performed in the frequency domain during the design process. The time histories of predicted vortex-induced moment obtained from the analysis were, therefore, converted to the frequency domain so that the results could be made usable with the conventional vessel-design process. Therefore, equation (42) in the text is taken to be a frequency-domain representation of the results in Figure 10 using a criterion of equivalent sinusoidal moment calculated from the plotted results as explained in Section 4.

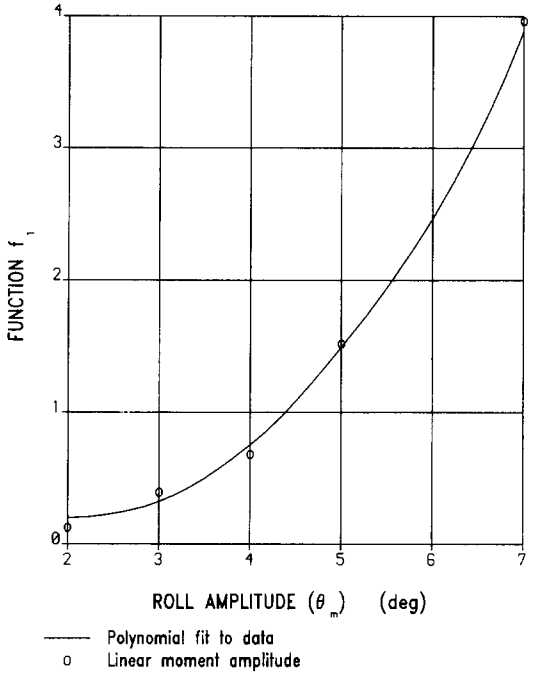

Figure 11. Vortex-shedding-induced moment-amplitude factor plotted against roll-motion amplitude (θ_m).

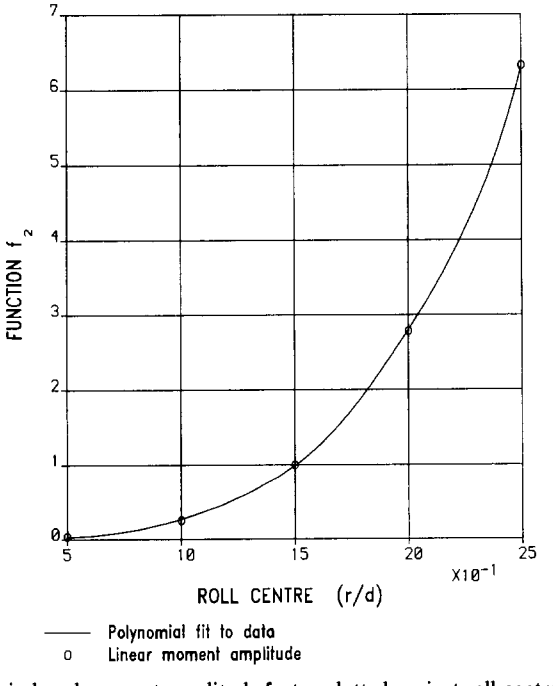

Figure 12. Vortex-shedding-induced moment-amplitude factor plotted against roll-centre-to-draught ratio (r/d).

4. Comparison with test data

Results are extracted here from a model test programme, separately reported by Brown et al. [17], to test the validity of results from the discrete-vortex model. A 1 : 36 scale Froude-number-scaled model barge of 2.400 m length and 0.800 m beam was used for the tests. The model had a total height of 0.240 m and was ballasted to a draught of 0.105 m. In order to measure wave-induced motions with and without large-scale flow separations, the model was fitted with two detachable keel-edge profiles; one being a right-angled "sharp" keel edge whereas the other was a rounded quadrant having a 40 mm radius of curvature.

Tests were carried out in long-crested regular and random waves in the 1.5 m deep, 18 m square wave basin at the Hydraulics Research Station, Wallingford. Measurements of model motions were performed using a pulley and potentiometer system to sense the three principal displacements and rotations about three perpendicular axes. Barge motions in surge, sway, heave, roll, pitch and yaw were sensed by twelve such potentiometers connected to the vessel by light nylon lines running to the tank sides and above the basin.

A data logger was used to acquire wave and motion data for long-crested regular and random seas at orientations corresponding to head seas, bow-quartering seas and beam seas. Regular-wave tests were carried out over a frequency range of 3 to 10 rad/s (3.8 to 12.6s full scale period) for wave heights from 25 to 40 mm (0.90 to 1.44 m full scale). Random-wave tests were performed with Pierson-Moskowitz wave spectra having characteristic frequencies of 5.0 to 9.8 rad/s (4.0 to 7.5 s full scale) and significant wave heights from 18 to 54 mm (0.65 to 1.94 m full scale).

Data for roll motions in beam seas only are presented in Figure 13 for rounded and sharp keel-edge profiles. The results demonstrate substantial differences between motions for the two keel-edge profiles. The roll natural frequency for the sharp keel-edge vessel is also slightly lower than the rounded. This is consistent with an effective increase in damping due to vortex shedding induced by the sharp keel edges. Figure 13 also shows linear potential-flow diffraction-theory estimates of barge roll motions taken from Brown et al. [17].

The differences between the results from potential-flow theory and the rounded and sharp keel-edge test data can be ascribed to a combination of three physical mechanisms. It is reasonable to suppose that tests with rounded keel-edge profile did not trigger any significant effects due to separation and consequent vortex shedding. The differences between the linear potential-flow theory and rounded-keel-edge must, therefore, be due to either skin friction or nonlinear wave loading. Furthermore, the differences between the data for rounded and sharp keel-edge profiles are likely to be entirely due to vortex-shedding effects. The comparisons with theory presented below are aimed at testing the latter hypothesis.

Including (42) in the vessel equation of roll motion and ignoring the effects of coupling with the sway mode gives

$$(I + I')\ddot{\theta}_{NL} + \beta\dot{\theta}_{NL} + S\theta_{NL} = W_a M_0 + M_{vs} \tag{45}$$

where the terms have their usual meanings, W_a being the wave amplitude, and M_0 the complex potential-flow wave exciting moment to a unit-amplitude wave. Ignoring sway motion is a justifiable assumption since the sway motions of a freely floating barge near roll resonance have been measured (see Brown et al. [17]), and the results indicate that the

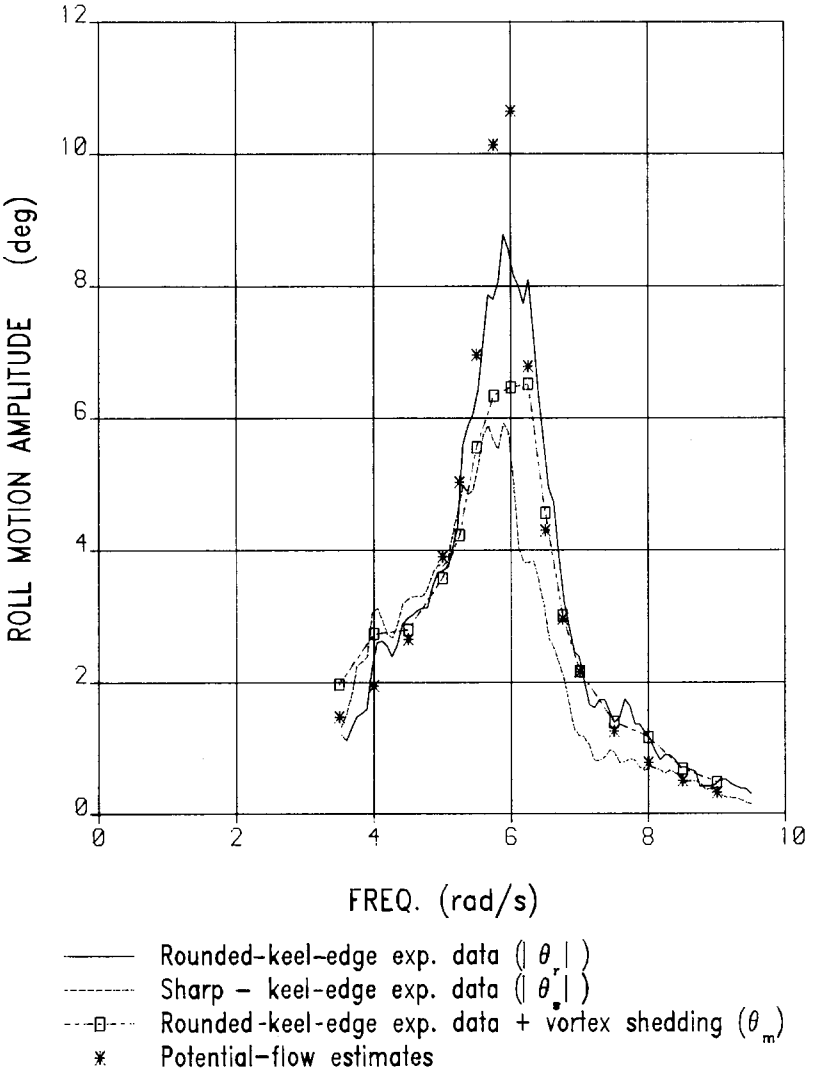

Figure 13. Theoretical estimates of reductions in roll due to vortex shedding applied to round-keel barge compared with sharp-keel results ($W_a = 1.9$ cm).

velocity induced near the corner due to sway motion is only about 15% of the velocity due to the vessel's roll motion. A time-series solution of (45) is possible but lengthy; hence the solution to a sinusoidal forcing function given by $M_{lvs}\exp(i\omega t)$ is developed. A simple criterion for the nonlinear contribution is the assume that the area A_m under the moment-variation-with-time curve is the same as that under an equivalent sinusoid of amplitude M_{lvs} giving

$$A_m = \int_0^{T_{pe}} |M_{vs}|\,dt = 2\int_0^{\pi/\omega} M_{lvs}\sin\omega t\,dt = \frac{4M_{lvs}}{\omega}$$

and hence

$$M_{\mathrm{lvs}} = \frac{\omega}{4}\int_0^{T_{\mathrm{pc}}} |M_{\mathrm{vs}}|\,\mathrm{d}t. \tag{46}$$

The linear representation allows harmonic solutions of the form

$$\theta_{\mathrm{NL}}\,\mathrm{e}^{\mathrm{i}\omega t} \tag{47}$$

where θ_{NL} is complex. Use of these results in (45) gives

$$\theta_{\mathrm{NL}} = \frac{W_{\mathrm{a}}M_0 + M_{\mathrm{lvs}}}{S - \omega^2(I+I') - \mathrm{i}\omega\beta} \tag{48}$$

which simplifies at resonance to

$$\mathrm{i}\omega\beta\theta_{\mathrm{NL}} = W_{\mathrm{a}}M_0 + M_{\mathrm{lvs}}. \tag{49}$$

Equations (48) and (49) can be solved using linear-theory results, allowing an estimate to be made of the complex roll amplitude θ_{NL} including nonlinear effects. The vortex-induced moment $\mathrm{M}_{\mathrm{lvs}}$ is now included in (48), giving

$$\theta_{NL} = \frac{W_{\mathrm{a}}M_{\mathrm{r}} + M_{\mathrm{lvs}}}{S - \omega^2(I+I') + \mathrm{i}\omega\beta}, \tag{50}$$

where θ_{NL} is the complex roll motion of the sharp-keel-edged vessel. The wave-exciting moment M_0 has been replaced here by M_{r} defined as the roll moment on the vessel ignoring coupling between sway and roll, but including the potential-flow wave-exciting moment and the moment due to skin friction and nonlinear wave loading. A good estimate of M_{r} may thus be obtained using the experimental data for the rounded-keel-edge motions, giving

$$\theta_{\mathrm{r}} = \frac{W_{\mathrm{a}}M_{\mathrm{r}}}{S - \omega^2(I+I') + \mathrm{i}\omega\beta} \tag{51}$$

where θ_{r} is the complex roll motion of the rounded-keel-edged vessel. Including this result in (50) gives

$$\theta_{\mathrm{NL}} = \theta_{\mathrm{r}} + \frac{M_{\mathrm{lvs}}}{S - \omega^2(I+I') + \mathrm{i}\omega\beta} \tag{52}$$

which can be solved assuming that the roll motions of the rounded- and sharp-keel-edged vessels are in phase with each other, and the vortex-induced moment acts to oppose barge roll motion. Roll-phase data calculated from the experimental tests on the sharp- and rounded-keel-edged barges presented in Figure 14 indicate that the roll motions of the two vessels are in phase with each other relative to the wave, and the results presented in Figure 10 indicate that the imposed moment does oppose the roll motions. Equation (52) may thus be written as

$$|\theta_{\mathrm{NL}}|\,\mathrm{e}^{\mathrm{i}(\omega t+\alpha_1)} = |\theta_{\mathrm{r}}|\,\mathrm{e}^{\mathrm{i}(\omega t+\alpha_1)} - \frac{f_1(\theta_{\mathrm{m}})f_2(r/d)\,\mathrm{e}^{\mathrm{i}(\omega t+\alpha)}}{S - \omega^2(I+I') + \mathrm{i}\omega\beta} \tag{53}$$

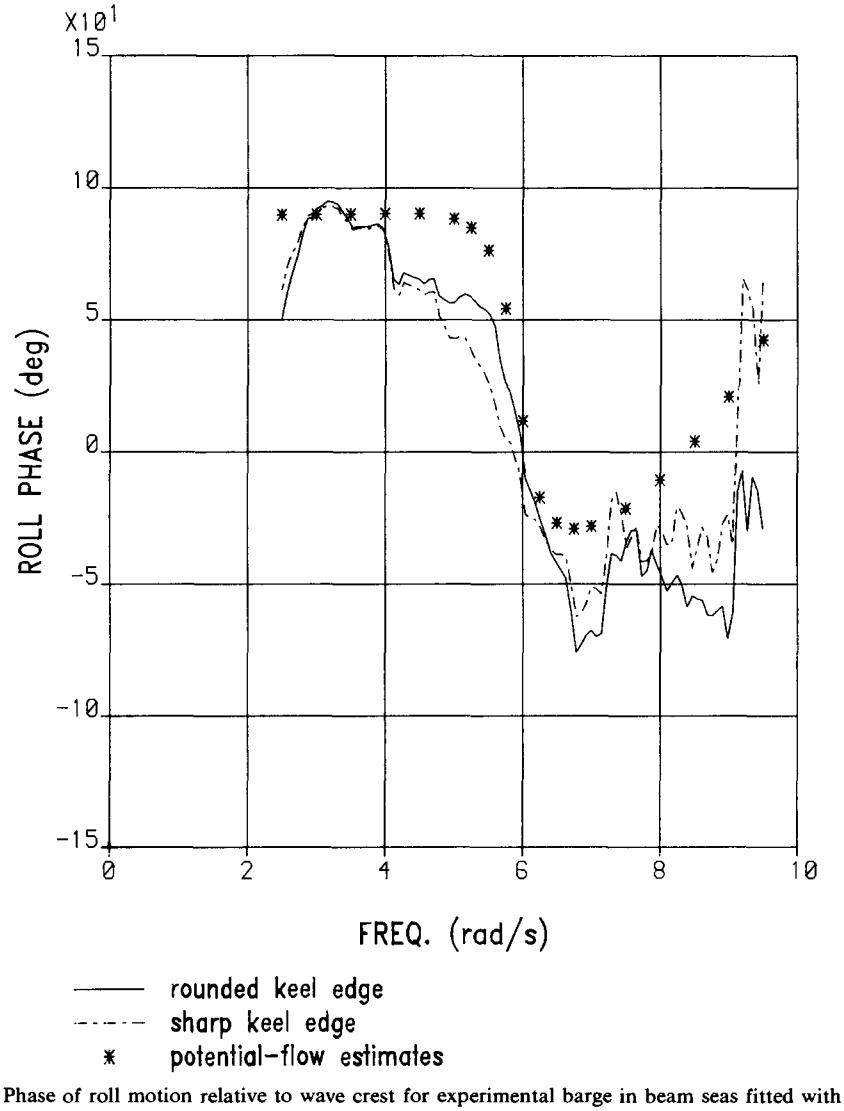

Figure 14. Phase of roll motion relative to wave crest for experimental barge in beam seas fitted with rounded and sharp keel edges, and calculated from potential-flow theory.

where α_1 is the phase of the rounded- or sharp-keel-edged vessel relative to the wave crest. Writing the denominator of the last term in this equation as $a + ib$ and noting that the complex roll amplitude $|\theta_{NL}|$ is given by θ_m allows simplification of (53) to

$$\theta_m = |\theta_r| - \frac{(a - ib)}{(a^2 + b^2)} f_1 f_2 \, e^{i(\alpha - \alpha_1)}$$

$$= |\theta_r| - \frac{f_1 f_2}{(a^2 + b^2)^{1/2}} e^{i(\alpha - \alpha_1 + \alpha_{ab})}, \tag{54}$$

where α_{ab} is the argument of $a - ib$. Equating the imaginary part of this expression to zero gives

$$\sin(\alpha - \alpha_1 + \alpha_{ab}) = 0 \tag{55}$$

and hence

$$\alpha = \alpha_1 - \alpha_{ab} + n\pi$$

where n is an integer. Solving for the real part gives

$$\theta_m = |\theta_r| - f_1 f_2/(a^2 + b^2)^{1/2}$$

which can be written as

$$(a^2 + b^2)^{1/2}\theta_m + f_1(\theta_m) f_2(r/d) - (a^2 + b^2)^{1/2}|\theta_r| = 0 \tag{56}$$

where

$$a = S - \omega^2(I + I')$$

and

$$b = i\omega\beta.$$

Equation (56) is quadratic in θ_m and can be solved assuming that the potential-flow values of roll-added inertia I' and damping apply, and that the roll-centre position r/d and rounded-keel-edge vessel-roll motions $|\theta_r|$ are known.

The resonant roll motion of the sharp-keel-edged barge θ_m is predicted from (56) and estimates of reductions in roll motions to regular waves caused by vortex shedding are presented in Table 1. The experimental values $|\theta_r|$ and $|\theta_s|$ indicate that the vessel fitted with sharp keel edges rolls as much as 54% less at resonance than that with rounded keel attachments, both vessels responding to identical sea states. The theoretical model of vortex shedding applied to the rounded-keel-edge wave-exciting roll-moment data as a starting point but using a roll-centre position of $r/d = 3.2$ (corresponding to that measured for the sharp-edged vessel) predicts roll motions that are in close agreement with the experimentally measured values for the sharp-keel-edged barge.

It is clear that calculation of roll-motion reductions due to vortex shedding requires knowledge of the roll-centre position for the vessel in the first place. However, the roll centre cannot be calculated unless the motions of the vessel, including the influence of vortices, are known. This problem is common in many areas of fluid mechanics where separate calculation of far-field inviscid flow and the near-field viscous flow leaves the interaction between the two to be included in the analysis. From a strictly academic viewpoint, the interaction needs to be included by incorporating the vortex-shedding effects (and those due to the non-linear loading mechanism described earlier) in an extended formulation of the diffraction problem. The motion response analysis that would follow from solution of the diffraction plus vortex-shedding forces could then be used to derive motions without prior knowledge of the roll-centre position.

However, in order to allow the vortex-shedding theory to be used in its present form, it

Table 1. Theoretical estimates of reductions in resonant roll motions due to vortex shedding

No.	Roll centre r/d	Wave freq. ω rad/s	Wave amp. W_a cm	$\lvert\theta_r\rvert$ deg	$\lvert\theta_s\rvert$ deg	γ_1	θ_m deg	γ_2
1	3.2	5.96	1.33	6.80	3.33	51.0%	3.21	52.8%
2	3.2	5.96	1.65	7.17	3.91	45.4%	3.29	54.0%
3	3.2	6.07	1.88	9.11	4.18	54.1%	3.68	59.6%
4	3.2	5.91	1.90	8.85	4.47	49.5%	3.64	58.8%

$\lvert\theta_r\rvert$ -rounded-keel-edge (HRS barge) roll-motion amplitude.
$\lvert\theta_s\rvert$ -sharp-keel-edge (HRS barge) roll-motion amplitude.
θ_m -rounded-keel-edge (HRS barge)+vortex-shedding adjustment roll-motion amplitude.

$$\gamma_1 = \frac{|\theta_r| - |\theta_s|}{|\theta_r|} \times 100\%, \quad \gamma_2 = \frac{|\theta_r| - \theta_m}{|\theta_r|} \times 100\%.$$

has been applied to the rounded-keel-edge wave-exciting roll-moment data as a starting point together with using a roll-centre position r/d of 1.4, corresponding to that measured from the rounded-keel-edge tests. This roll-centre position is expected to be close to the value that would arise from potential-flow theory.

The roll-motion reductions obtained for this case are presented in Figure 13. Theory predicts a reduction in resonant roll motions of 28% due to the presence of vortices whereas measured resonant-roll motions for the sharp-keel-edged vessel are 33% less than the rounded-keel-edge values. Away from resonance, the experimental data are in reasonable agreement with each other and with predicted values since vortex shedding and nonlinear effects are small due to the much decreased roll amplitude here.

The results presented above indicate that, for the purpose of engineering design, roll-centre estimates obtained from potential-flow theory can be used for the vortex-shedding theory. This procedure will yield a sufficiently accurate roll-motion prediction.

It is concluded from the results of Table 1 and Figure 13 that the discrepancy in measured resonant roll motions for rounded- and sharp keel-edged-vessels can be almost entirely accounted for by the forces due to vortex shedding. The coupling between far-field inviscid flow and the near-field viscous flow arises within a requirement for an accurate roll-centre position for computing the viscous forces.

References

[1] W. Froude, On, the resistance in rolling of ships, *Naval Science* 3 (1874) 312.
[2] M. Martin, Roll damping due to bilge keels, Iowa Inst. of Hydraulic Research, Contract Nonr. 1611 (01), Nov. 1958.
[3] Sir W. White, Notes on further experience with first class battleships, *Trans. Inst. Nav. Arch.* 36 (1895) 127.
[4] G.H. Bryan, The action of bilge keels, *Trans. Inst. Nav. Arch.* 42 (1900) 198.
[5] R.W.L. Gawn, Rolling experiments with ships and models in still water, *Inst. Nav. Arch.* 82 (1940).
[6] J.F. Dalzell, A note on the form of ship roll damping, *J. Ship Research* 22 (1978) 178–185.
[7] H. Kato, On the frictional resistance to rolling of ships, *Soc. Nav. Arch. Japan* 102 (1958) 115.
[8] N. Tanaka, A study on bilge keels (Pt. 4, On the eddy-making resistance to the rolling of a ship hull), *Soc. Nav. Arch. Japan* 109 (1960) 205–212.

[9] N. Salvesen, E.O. Tuck and O. Faltinsen, Ship motions and sea loads, *Trans. Soc. Nav. Arch. Marine Engrs.* 78 (1970) 421.
[10] Y. Ikeda, Y. Himeno and N. Tanaka, A prediction method for ship roll damping, Dept. of Nav. Arch., Univ. of Osaka, Japan, Rep. 00405 (1978).
[11] J.N. Newman, *Marine hydrodynamics*, MIT Press, 2nd edn. (1978).
[12] Y. Ikeda, Y. Himeno and N. Tanaka, On eddy making component of roll damping force on naked hull, *J. Soc. Nav. Arch. Japan* 142 (1977) 54.
[13] J.A. Keuning and W. Beukelman, Hydrodynamic coefficients of rectangular barges in shallow water, Paper 55, BOSS'79, Imperial Coll. Sci. Tech. London (1979) 105–124.
[14] W.P. Stewart, W.A. Ewers and P.J. Denton, Nonlinear barge motion response. Use of physical models in the design of offshore structures, Paper 23, Garston, Watford, England (1979).
[15] P. Kaplan, C.W. Jiang and J. Bentson, Hydrodynamic analysis of barge-platform systems in waves. RINA Spring Meeting, Paper 8, (1982).
[16] J.-P.F. Denise, On the roll motion of barges, *RINA Supplementary Paper* 125 (1983) 255.
[17] D.T. Brown, R. Eatock Taylor and M.H. Patel, Barge motions in random seas – a comparison of theory and experiment, *J. Fluid Mech.* 129 (1983) 385–407.
[18] L. Rosenhead, Formulation of vortices from a surface of discontinuity, *Proc. Roy. Soc.* 134 (1931) 170–192.
[19] G.D. Birkhoff and J. Fisher, Do vortex sheets roll up?, *Rendi. Circ. Math. Palermo* 8 (1959) 1077.
[20] F.R. Hama and E.R. Burke, On the rolling up of a vortex sheet, Univ. of Maryland Tech. Note BN-220, USA (1960).
[21] F.H. Abernathy and R.E. Kronauer, The formation of vortex streets, *J. Fluid Mech.* 13 (1962) 1–20.
[22] F.L. Westwater, The rolling up of the surface of discontinuity behind an aerofoil of finite span, R. and M. 1692, Aero. Research Council, GB (1935).
[23] H. Kaden, Aufwicklung einer unstabilen Unstetigkeitsflache, *Ing. Arch.* 2 (1931) 140–168.
[24] D.W. Moore, The discrete vortex approximation of a finite vortex sheet, Cal. Inst. Tech. Rep., AFOSR, USA (1971) 1804–1869.
[25] R.R. Clements, An inviscid model of two-dimensional vortex shedding, *J. Fluid Mech.* 57 (1973) 321–336.
[26] R.R. Clements and D.J. Maull, The representation of sheets of vorticity by discrete vortices, *Prog. Aerospace Sci.* 16 (1975) 129–146.
[27] K. Kuwahara, Numerical study of flow past an inclined flat plate by an inviscid model, *J. Phys. Soc. Japan* 35 (1973) 1545–1551.
[28] T. Sarpkaya, Inviscid model of two-dimensional vortex shedding for transient and asymptotically steady separated flow over an inclined plate, *J. Fluid Mech.* 68 (1975) 109–128.
[29] L.M. Milne-Thomson, *Theoretical hydrodynamics*, Macmillan & Co., 5th edn., (1968).
[30] P.T. Fink and W.K. Soh, Calculation of vortex sheets in unsteady flow and applications in ship hydrodynamics, *Proc. 10th Symp. Naval Hydrodynamics*, Cambridge, Massachusetts, USA, (1974) 463–491.
[31] P.K. Stansby, An inviscid model of vortex shedding from a circular cylinder in steady and oscillatory far flows, *Proc. Inst. Civ. Engrs.* 63 (1977) 865–880.
[32] T. Sarpkaya and R.L. Schoaff, Inviscid model of two-dimensional vortex shedding by a circular cylinder, *AIAA J.* 17 (1979) 1193.
[33] M. Efthymiou and R. Narayanan, Current induced forces on submarine pipelines – a discrete vortex model, *Proc. Inst. Civ. Engrs.* 73 (1982) 109–123.
[34] M.H. Longuet Higgins Oscillating flow over steep sand ripples, *J. Fluid Mech.* 107 (1981) 1–35.
[35] P.W. Bearman, J.M.R. Graham, P. Naylor and E.D. Obasaju, The role of vortices in oscillatory flow about bluff cylinders, *Proc. Int. Symp. Hydrodynamics in Ocean Engng.*, NIT Trondheim, Norway (1981).
[36] J.M.R. Graham, The forces on sharp edged cylinders in oscillatory flow at low Keulegan-Carpenter numbers, *J. Fluid Mech.* 97 (1980) 331–346.
[37] P.W. Bearman, M.H. Downie and J.M.R. Graham, Calculation method for separated flows with application to oscillatory flow past cylinders and roll damping of barges, Unpublished report, Imperical Coll. Sci. Tech. London (1983).
[38] O.M. Faltinsen and B. Pettersen, Vortex shedding around two-dimensional bodies at high Reynolds number. *Proc. 14th Symp. on Naval Hydrodynamics,* Univ. of Michigan, Ann Arbor, USA, (1982).
[39] A. Pope, *Basic wing and airfoil theory*, McGraw-Hill Book Comp., New York, 1st edn. (1951).
[40] L. Landweber and C.S. Yih, Forces, moments and added masses for Rankine bodies, *J. Fluid Mech.* 1 (1956) 319–336.
[41] P.K. Stansby, A numerical study of vortex shedding for one or two cylinders, *Proc. European Mech. Colloq.*, London, No. 119, 1979.